engineering proceedings

Proceeding Paper

Off-the-Shelf Simulation for Demoldable Mandrels: An Experimental and Numerical Approach to Thermoplastic Shape-Memory Polymers [†]

Fabian Flüh [1,*], Parth Shingte [1], Óscar Ludeña Navarro [1] and Jonas Wermter [2]

[1] German Aerospace Center (DLR), Institute of Lightweight Systems, 38108 Braunschweig, Germany; parth.shingte@dlr.de (P.S.); oscar.ludenanavarro@dlr.de (Ó.L.N.)
[2] Institute for Plastics Processing in Industry and Craft at RWTH, Aachen University (IKV), 52074 Aachen, Germany; jonas.wermter@ikv.rwth-aachen.de
[*] Correspondence: fabian.neumann@dlr.de
[†] Presented at the 15th EASN International Conference, Madrid, Spain, 14–17 October 2025.

Abstract

The production of one-piece composite hollow profiles with undercuts presents significant challenges to conventional mold concepts. Mandrels made of thermoplastic shape-memory polymers could facilitate demolding and reduce tooling costs. To design molds in a commercial environment, it is critical to determine their behavior using off-the-shelf Finite Element Analysis (FEA) software Ansys 2024R1. This study presents a shape-memory test procedure for coupon test specimens under tensile load. Furthermore, the test is used to validate a simulation using a generalized Maxwell model, a linear viscoelastic material model implemented in off-the-shelf commercial FEA software Ansys 2024R1. The material investigated is amorphous PET. The simulation shows good results in comparison with the thermo-mechanical shape-memory test. The results are then transferred to blow-molded bottle-shaped mandrels, e.g., for the manufacturing of Type V pressure vessels. Test results are compared with the simulation results and deviations are discussed. In conclusion, the straightforward "from material to solution" approach presented allows us to model and simulate the shape-memory behavior of linear viscoelastic polymers with off-the-shelf commercial FEA software.

Keywords: shape-memory polymer (SMP); time–temperature superposition (TTS); viscoelastic model; parameter identification; mandrel; finite element analysis (FEA)

1. Introduction

Fiber-reinforced polymer (FRP) composites are widely used in aerospace because of their fatigue resistance and excellent tailorable material properties. FRP makes up approximately 50% of the structural mass in modern commercial aircraft such as the Airbus A350 and Boeing 787, and constitutes more than 90% in General Aviation and UAV structures. Demand for FRP parts is expected to rise with hydrogen powered vehicles, where pressure vessel production is a key growth area. Meeting this demand requires highly automated manufacturing processes, but the production of complex hollow profiles with smooth inner surfaces and undercuts (e.g., struts, air intakes, Type V pressure vessels) remains difficult for conventional tooling methods.

Suitable automated manufacturing methods include filament or towpreg winding, automated fiber placement (AFP), and braiding. Reusable mandrels that are rigid at room

Academic Editors: Spiros Pantelakis, Andreas Strohmayer and Gustavo Alonso

Published: 5 May 2026

 https://doi.org/10.3390/engproc2026133069

temperature during preforming and become demoldable after curing require either a shape change or a material property shift. Shape-memory polymers (SMPs) that exhibit a temperature triggered shape-memory effect offer this capability. SMP mandrels could enable the manufacturing of one piece, Type V pressure vessels or s-shaped air intakes without the need for soluble or meltable mandrels with dirt-associated demolding processes. However, research on thermoplastic SMPs for tooling is scarce, and no studies have addressed the shape-memory effect in blow molded cores [1].

1.1. Constitutive Models of SMP

Three established methods for constitutive models can be found in the literature: (1) rheological models, (2) phase transition models, and (3) unit cell-based multi-branch models. Additionally, new model-building methods have emerged that replace fitting parameters with physics-based parameters, combine different SMP models, or incorporate multiple algorithms and functions [2]. Rheological models for SMP are phenomenological viscoelastic and viscoelastic–plastic models. These models consist of three main elements that represent the behavior of polymer chains at the macroscopic level: (1) elastic springs, (2) viscous dashpots and (3) slip elements. Diani et al. [3] made significant advances by using a generalized Maxwell or Maxwell–Wiechert model (GMM), which recognizes that relaxation occurs over a distribution of times rather than at a single time, as well as the Williams–Landel–Ferry (WLF) equation to describe the relationship between relaxation time and temperature.

1.2. Implementation in FEA Software

Since rheological models are relatively easy to solve, the GMM and the WLF equation, along with Simo's finite strain extension of the generalized Maxwell model, are available in commercial finite element analysis (FEA) software, such as ABAQUS 2024 and ANSYS 2023R2 [4]. This facilitates the integration of viscoelastic shape-memory behavior in simulations [5].

1.3. Aim of This Work

This work aims to provide an easy-to-follow guideline to cost-effective and time-efficient implementation of the linear viscoelastic shape-memory effect of thermoplastic polymers in commercial FEA programs using fully open-source and transparent methods. The aim of the proposed methods is not to be as accurate as possible in predicting the shape-recovery process but to offer an as-good-as-necessary approach to the prediction of shape fixity and shape recovery rate for engineering applications as shape-memory mandrel design.

2. Materials & Methods

The necessary material parameters for implementing shape-memory behavior in standard FEA software can be obtained using the methods described in this chapter. The overall workflow for parameter identification used in this work is shown in Figure 1 and was elaborated in our previous work [6]. Table 1 lists the thermoanalytical equipment used for parameter identification.

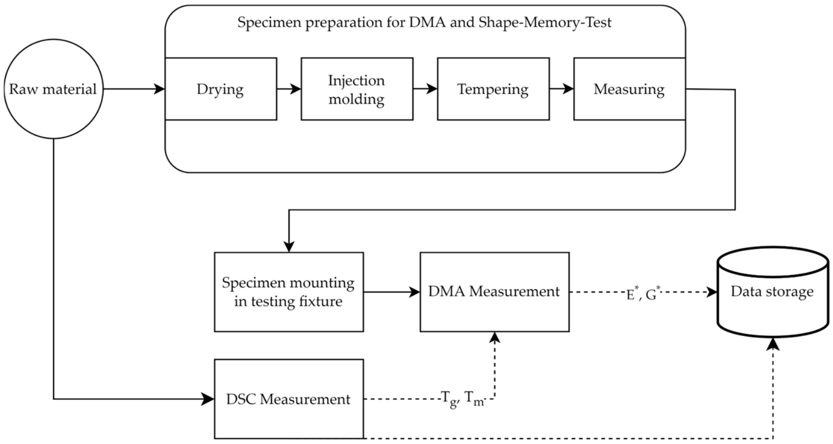

Figure 1. Schematic representation of the parameter identification workflow.

Table 1. Methods and equipment used for thermoanalysis.

Method	Equipment	Parameters
Specimen preparation	HAAKE™ MiniJet Pro (Thermo Fisher Scientific Inc., Waltham, MA, USA)	Cylinder: 250 °C Mold: 30 °C Pressure: 300 bar
DSC	DSC 2 TOPEM (Mettler Toledo Inc., Columbus, OH, USA)	25 °C ... 290 °C; 10 K/min
DMA	MCR 702 (Anton Paar Group AG, Graz, Austria)	73 °C ... 94 °C; 0.1 Hz ... 10 Hz

2.1. Polymers

In our previous work we identified PET as a favorable material for mandrel production [7]. In this work LUMEX A is used as the material, supplied as an extruded film with 0.5 mm thickness.

2.2. Thermoanalytical Measurements

The PET samples are scanned using a Mettler DSC 2 TOPEM (Mettler Toledo Inc., Columbus, OH, USA) from 25 °C to 290 °C at 10 K/min. Two heating cycles and one cooling cycle are recorded. Dynamic mechanical analysis (DMA) is used to determine the temperature and frequency dependent complex shear and elastic moduli, according to Rodriguez Agudo et al. [8]. An Anton Paar MCR 702 rheometer (Anton Paar Group AG, Graz, Austria) equipped with a linear drive and a solid rectangular fixture (SRF) is used. Frequency sweeps from 0.1 Hz to 10 Hz are performed at discrete temperature steps from 73 °C to 94 °C in 3 °C increments.

2.3. Material Parameter Identification

First, a master curve is constructed, applying the time–temperature superposition (TTS) principle. Therefore, the optimization algorithm published by Lennon et al. is applied, using the mastercurves 0.2.3 Python package provide by the beforementioned authors [9,10]. To interpolate between experimental acquired data at the discrete temperature steps, the Williams–Landel–Ferry (WLF) shift function is used. This requires fitting the function to the shift factors obtained from the master curve construction. Fitting the parameters is done by a Python 3.12 script using the suggested values by Williams et al. as start points [11].

Next, the complex modulus Prony series, a representation of the elements in the GMM, is fitted to the master curve data.

2.4. Shape-Memory Testing

2.4.1. Shape-Memory Coupon Test

A shape-memory test is performed to verify the simulation model. PET coupons are mounted in the Anton Paar MCR 702 rheometer equipped with a linear drive. The coupons are stretched to 2% strain at 90 °C. Then, the specimen is cooled to 65 °C and the clamping force is released. Subsequently, the specimen is heated to 95 °C and the recovery process is tracked. The test follows the setup previously published by us [6].

2.4.2. Shape-Memory Mandrel Test

To validate the 3D geometry transferred simulation results, a blow molded specimen are necessary. These specimens are stretch blow molded using the laboratory size stretch blow molding machine of the Institute for Plastics Processing in Industry and Craft at RWTH Aachen University. PET preforms of 2 mm wall thickness and 100 m length by HUSKY Technologies are used. Comparability with the LUMEX A from coupon testing is ensured through DSC and DMA measurements. The preforms are stretched at 95 °C to be in line with the coupon shape-memory test. After forming, the bottle-shaped specimens are heated in an oven to 120 °C and volume is measured after recovery. This test procedure was already demonstrated in our previous work [12].

3. Results

3.1. Results of Thermo-Mechanical Testing

The DSC results are shown in Table 2. The results of the frequency sweeps at discrete temperature steps of the PET coupon are shown in Figure 2.

Table 2. Summarized results of the DSC.

Measurand	PET
T_g	82.79 °C
T_m	248.16 °C
T_c	165.12 °C

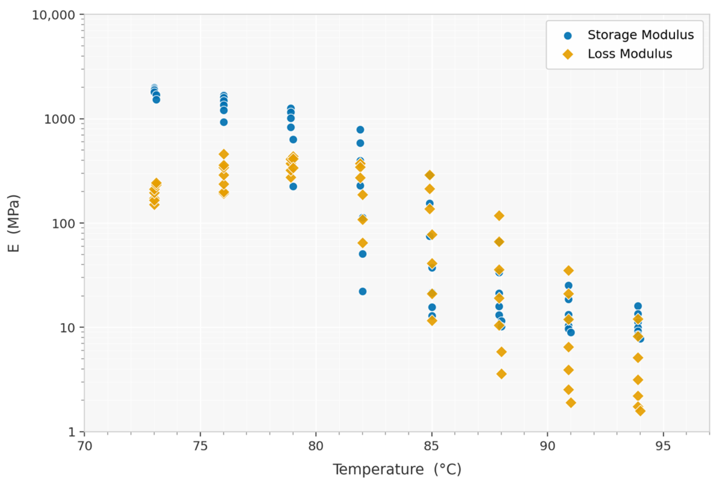

Figure 2. Raw data of storage and loss modulus over temperature.

3.2. Parameter Identification and Implementation in FEA Software

The identification of the WLF parameters and Prony series parameters is done as described in Section 2.3 using the Python scripts made publicly available by us [13]. The fitted WLF parameters are C1 = 9.815, C2 = 33.283 at the reference temperature T_{ref} = 82 °C. The fitted Prony curve is shown in Figure 3. The fit matches the measured data well.

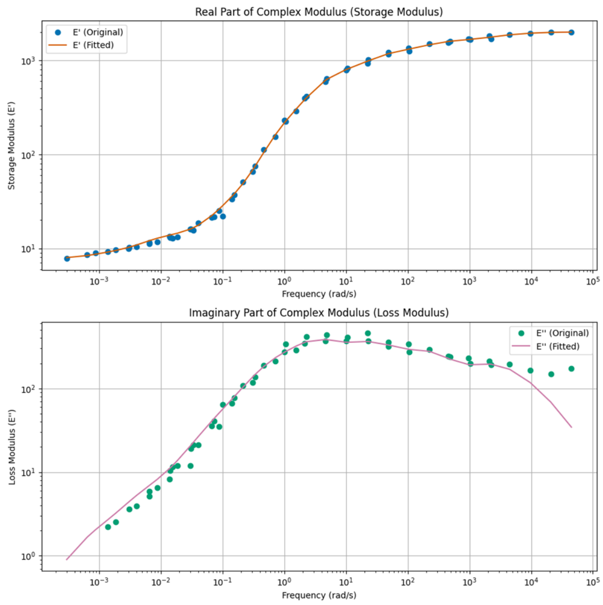

Figure 3. Master curves of the storage modulus (**upper** plot) and loss modulus (**lower** plot).

3.3. FEA Implementation of the Shape-Memory Test

To validate the extracted parameters, a coupon tensile test is carried out following the methods described in our previous work [6]. The simulation shows good correlation with the shape-memory coupon test carried out with 2% strain. The measured shape fixity ratio is 93.6%. The simulation predicts 98.9%. The measured shape recovery ratio is 92.6%, while 94.3% are predicted by simulation. The shape recovery ratio error is 1.7%. To transfer these results to 3D geometries, the Stretch Blow Molding process is simulated in ANSYS 2024R1 Polyflow. This blow molding simulation is used to obtain the thickness distributions and the extension or stretch components for the final geometry with respect to the preform. A python script is written to read corresponding stress values from a biaxial stress–strain curve. The biaxial tension test data was taken from Teng et al. [14]. In the Transient Structural module, the data is imported as an initial stress load. The final geometry of the bottle is imported as a shell for the shape recovery simulation. A cylindrical coordinate system is introduced on the geometry. This allows for the import of stress components directly, instead of converting the components to the cartesian coordinates. The stress tensor at each node from the Polyflow mesh is mapped to the structural. To include the effect of thickness variation along the geometry of the bottle on the shape recovery, the thickness outputs from Polyflow are also mapped to the structural shell midsurface. The mapped data is validated using the validation feature and no significant errors or deviations are observed.

3.4. Shape-Memory Simulation Results

Figure 4a illustrates the thickness distribution obtained from the blow molding simulation. The stress tensor components at each node are mapped onto the structural mesh elements using the Triangulation weighting method. The equivalent von Mises stress contour after mapping is shown in Figure 4b. The base region shows the highest stress values with local maxima reaching approximately 60–65 MPa. This correlates to the high thinning as observed in the thickness distribution. Stress vectors in the axial and tangential direction are also observed to be larger at the base region of the bottle. This corresponds to the high axial and tangential stretch values in this region. On the walls of the bottle, moderate stress values in the range of 20–35 MPa are observed. Overall, the mapped stress field correlates well with the thickness distributions and extension components. Regions with high stretch values correspond to elevated stresses, while areas with low stretch values correspond to low stresses. This correlation validates the stress mapping procedure, meaning that the obtained initial stress field can be a good starting point for stress relaxation and creep simulations.

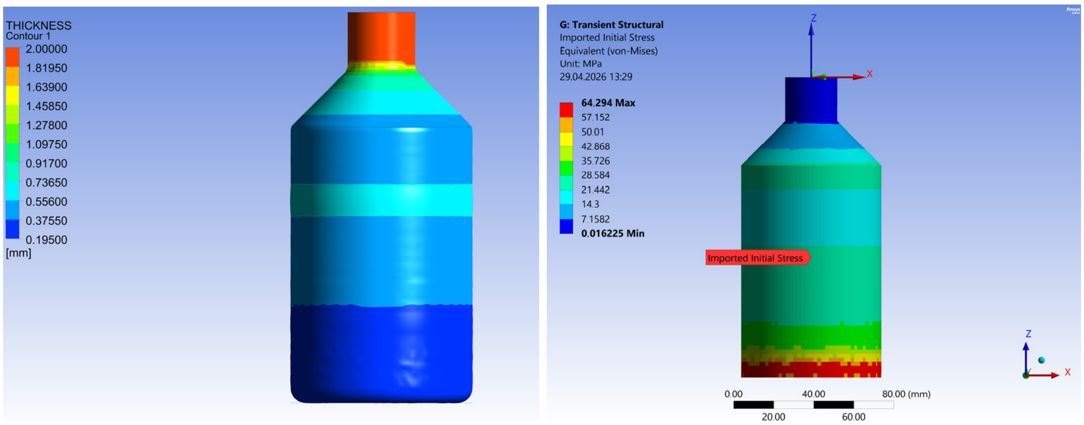

(**a**) (**b**)

Figure 4. (**a**) Thickness distribution from the Polyflow blow-molding simulation; (**b**) equivalent von Mises stress after mapping in Mechanical.

An initial investigation into post-forming shape recovery was conducted using an implicit transient structural analysis. However, the implicit solver proved unable to reproduce the expected recovery behavior. When the stresses obtained from the forming simulation were mapped onto the structural mesh, their magnitudes decreased sharply during the first equilibrium iterations. The solver, in an attempt to equilibrate the imported stress field, caused the stress field to artificially concentrate at the bottom region of the bottle. Although these redistributed stresses subsequently decayed in accordance with the prescribed viscoelastic relaxation time constants, the global deformation of the bottle remained essentially unchanged. An attempt was made to import the strain field instead, but the solver was unable to converge under such large strain magnitudes. Since only a single step initial strain field application is permitted, it was not possible to incrementally ramp the strains for solution stability.

4. Discussion and Conclusions

The described methods for modeling the shape-memory behavior of thermoplastic polymers showed good correlation with the results of coupon tensile tests within the linear viscoelastic range of the material. However, these results have already been discussed for PA6 in our previous work [6]. For PET, the same limitations and errors are applicable. This work proved the transferability of the previous results to other thermoplastics polymers such as PET. While shape fixity and recovery ratio as well as recovery time can be simulated using the simple GMM with good correlation to the test results, the actual path of recovery shows some deviation. Since our research is focused on deformable mandrels, this deviation is neglectable for our use-case, but could limit the method with regard to other applications. Transferring these results to 3D blow molded geometries has challenges in terms of solving the imported stresses and deformations in a transient simulation. The observations indicate that accurate shape-recovery predictions require preservation of the complete internal state variables generated during the forming process. These variables are not preserved through a stress mapping within a conventional implicit formulation in ANSYS 2024R1. Therefore, using an explicit solver could overcome the limitations encountered in this study.

5. Outlook

A new step forward in this research has been initiated, focusing on physics-informed neural networks (PINNs) and data-driven material models as surrogate constitutive laws for PET above its glass transition temperature. Building on the calibrated GMM with WLF shifting and its implementation in commercial FE software Ansys 2024R1, the next objective is to replace the closed-form viscoelastic relation by a neural network that follows the same interface as a convectional user material subroutine. The proposed route for developing the surrogate constitutive model is summarized in Figure 5.

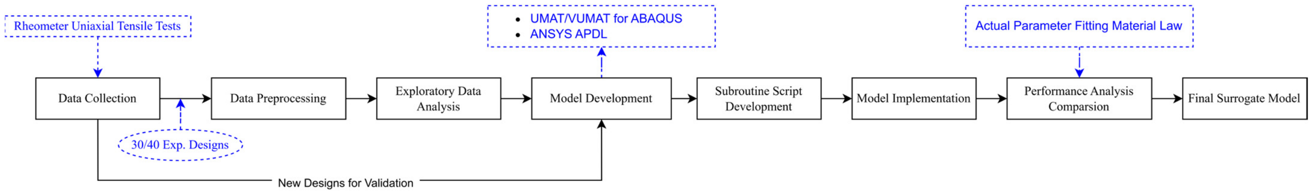

Figure 5. Process flowchart for surrogate constitutive model development.

Following the multiaxial PET characterization strategy reported by Teng et al. [14], the training data have been collected in the lab as experimentally measured stress–strain-time curves at various prescribed strain levels, strain rates and temperatures above the glass transition. The network will receive temperature, time increment, strain increment and current stress state as inputs and return the corresponding stress increment, so that it can be embedded seamlessly into a finite element framework, as illustrated in Figure 6. Inspired by the thermodynamics-based PINN formulation of Rezaei et al. [15], the PET constitutive equations and dissipation constraints will be embedded as physics residuals in the loss function. In this way, the resulting PET surrogate model is expected to reduce computational cost in parametric studies and design loops while maintaining, or even improving, predictive accuracy.

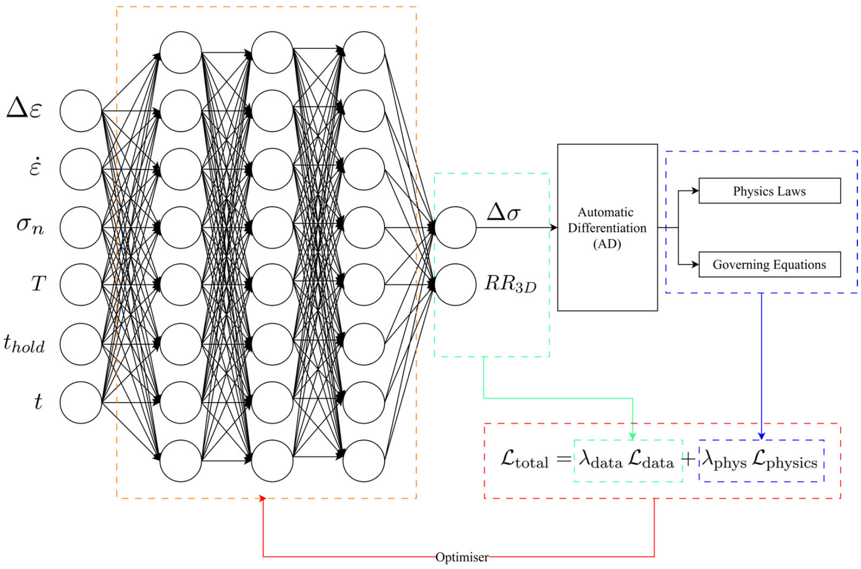

Figure 6. Proposed PINN-based surrogate constitutive modeling framework for PET.

Author Contributions: Conceptualization, F.F.; methodology, F.F., P.S. and Ó.L.N.; software, F.F. and P.S.; validation, F.F. and P.S.; investigation, F.F., P.S., Ó.L.N. and J.W.; resources, F.F. and J.W.; data curation, F.F., P.S., Ó.L.N. and J.W.; writing—original draft preparation, F.F., P.S., Ó.L.N. and J.W.; writing—review and editing, F.F., P.S. and Ó.L.N.; visualization, F.F., P.S. and Ó.L.N. All authors have read and agreed to the published version of the manuscript.

Funding: The research was carried out within the framework of the German Aerospace Center's core funded research.

Institutional Review Board Statement: Not applicable.

Informed Consent Statement: Not applicable.

Data Availability Statement: The data presented in this study are available upon request from the corresponding author.

Conflicts of Interest: The authors declare no conflicts of interest. The funders had no role in the design of the study; in the collection, analyses, or interpretation of data; in the writing of the manuscript; or in the decision to publish the results.

References

1. Neumann, F. Variable Shape Tooling for Composite Manufacturing: A Systematic Review. *J. Compos. Sci.* **2024**, *8*, 131. [CrossRef]
2. Yan, C.; Li, G. Tutorial: Thermomechanical constitutive modeling of shape memory polymers. *J. Appl. Phys.* **2022**, *131*, 111101. [CrossRef]
3. Diani, J.; Gilormini, P.; Frédy, C.; Rousseau, I. Predicting thermal shape memory of crosslinked polymer networks from linear viscoelasticity. *Int. J. Solids Struct.* **2012**, *49*, 793–799. [CrossRef]
4. Simo, J.C. On a fully three-dimensional finite-strain viscoelastic damage model: Formulation and computational aspects. *Comput. Methods Appl. Mech. Eng.* **1987**, *60*, 153–173. [CrossRef]
5. Azzawi, W.A.; Epaarachchi, J.A.; Islam, M.; Leng, J. Implementation of a finite element analysis procedure for structural analysis of shape memory behaviour of fibre reinforced shape memory polymer composites. *Smart Mater. Struct.* **2017**, *26*, 125002. [CrossRef]
6. Neumann, F.; Cerbe, F.; Sinapius, M. From Material to Solution: Implementing Shape Memory Behavior of Thermoplastic Polymers in Commercial FEA Software for Structural Analysis. *J. Manuf. Mater. Process.* **2025**, *9*, 73. [CrossRef]
7. Neumann, F.; Rings, B.; Golombek, H.L. Investigation of thermoplastic polymers with regard to their suitability as mold material in the FRP manufacturing process. In Proceedings of the DLRK 2023, Stuttgart, Deutschland, 19–21 September 2023.
8. Rodríguez Agudo, J.A.; Haeberle, J.; Müller-Pabel, M.; Troiss, A.; Shetty, A.; Kaschta, J.; Giehl, C. Characterization of the temperature and frequency dependency of the complex Poisson's ratio using a novel combined torsional-axial rheometer. *J. Rheol.* **2023**, *67*, 1221–1250. [CrossRef]
9. Lennon, K.R.; McKinley, G.H.; Swan, J.W. A Data-Driven Method for Automated Data Superposition with Applications in Soft Matter Science. *arXiv* **2022**. Available online: http://arxiv.org/pdf/2204.09521 (accessed on 29 April 2026). [CrossRef]
10. Lennon, K.R.; Swan, J.W. Automatic Identification of Similarity Relations. Massachusetts Institute of Technology. Available online: https://github.com/krlennon/mastercurves/blob/main/CITATION.cff (accessed on 29 April 2026).
11. Williams, M.L.; Landel, R.F.; Ferry, J.D. The Temperature Dependence of Relaxation Mechanisms in Amorphous Polymers and Other Glass-forming Liquids. *J. Am. Chem. Soc.* **1955**, *77*, 3701–3707. [CrossRef]
12. Neumann, F.; Rings, B.; Golombek, H. Investigation of the Shape-Memory Capabilities of Stretched Thermoplastic Polymers for Mandrel Production. In Proceedings of the SAMPE 2024 Conference and Exhibition, Long Beach, CA, USA, 20–23 May 2024. [CrossRef]
13. Neumann, F. *DMA-MaWProFit: Identify WLF-Equation and Prony Series Parameters from Frequency Domain DMA Test Data for Visco-Elastic Materials*; Zenodo: Genève, Switzerland, 2024. [CrossRef]

14. Teng, F.; Menary, G.; Malinov, S.; Yan, S.; Stevens, J.B. Predicting the multiaxial stress-strain behavior of polyethylene terephthalate (PET) at different strain rates and temperatures above Tg by using an Artificial Neural Network. *Mech. Mater.* **2022**, *165*, 104175. [CrossRef]
15. Rezaei, S.; Moeineddin, A.; Harandi, A. Learning solutions of thermodynamics-based nonlinear constitutive material models using physics-informed neural networks. *Comput. Mech.* **2024**, *74*, 333–366. [CrossRef]